Hollow metal island films as plasmonic sensors produced by galvanic replacement

Ivana Fabijanić[a], Maja Mičetić[a], Matej Bubaš[a], Vesna Janicki[a], Sigrid Bernstorff[b], Jordi Sancho-Parramon[a,*]

[a] *Ruđer Bošković Institute, Bijenička cesta 54, Zagreb 10000, Croatia*
[b] *Elettra-Sincrotrone Trieste S.C.p.A., Strada Statale 14 km, 163.5 in AREA Science Park, Basovizza/Trieste 34149, Italy*

Abstract

Hollow nanoparticles show enhanced plasmonic response with respect to their solid counterparts. Formation of hollow nanostructures is usually carried out in nanoparticle solutions via galvanic replacement and Kirkendall effect driven by the redox potential difference between metals of a redox couple. In this work the formation of hollow nanoparticle layers using metal island films fabricated by physical vapor deposition as templates is demonstrated. Ag metal island films on glass and silicon substrates are titrated with a solution containing tetrachloroauric acid as oxidizing agent. The islands morphology and their plasmonic properties gradually change with the increase of titration solution concentration due to the effects of galvanic replacement. In comparison to untreated samples, a four-fold enhancement of the refractive index sensitivity factor (360 nm/RIU vs 92 nm/RIU) and two and a half times increase of the figure of merit (1.37 vs 0.56) are observed for hollow island films obtained with large titration concentration. The presented approach merges the advantages of large area coverage and high particle density of island films with the plasmonic properties of hollow nanoparticles in a straightforward way that is suitable for cost-effective fabrication of plasmonic sensors.

Keywords: hollow nanoparticles, plasmonics, metal islands, refractive index sensors, galvanic replacement

1. Introduction

Hollow structures play a central role in nanotechnology thanks to the wide range of applications enabled by their unique properties. It has been shown that their characteristic large surface to volume ratio, low density and diverse

*Corresponding author
Email address: jsancho@irb.hr (Jordi Sancho-Parramon)

functionality associated to multiple shells are advantageous for drug delivery, energy storage and catalysis [1, 2, 3]. In the field of nanophotonics, hollow metal nanoparticles are a cornerstone for the development of plasmonics. Their electromagnetic response is governed by the hybridization between cavity and particle modes into bonding and anti-bonding plasmon resonances [4]. The properties of these hybrid resonances can be widely tailored well beyond the limits of solid nanoparticles by controlling the particle geometry [5]. Adjusting the plasmon resonance of gold nano-shells into the near-infrared window of biological tissues represents a canonical example of this tuning ability with many applications in biomedicine [6, 7, 8]. Plasmon resonances in hollow nanoparticles are highly sensitive to environment modifications and hence can be used for label-free optical sensing [9]. Large enhancement and spatial distribution of electromagnetic near field in hollow nanoparticles are also favorable properties for Raman spectroscopy [10] and photocatalytic activity [11] applications.

Hard and soft templating synthesis methods have been extensively used to fabricate hollow metal nanostructures [1]. Essentially, these approaches consist of coating an auxiliary template with a metal shell and the successive template removal. Alternatively, conversion chemistry has emerged as a versatile approach for self-templating synthesis of hollow nanostructures with precise composition and morphology control [12]. Galvanic replacement is a straightforward conversion chemistry route based on the difference in the electrochemical potential between the sacrificial metal template and a more noble metal ion in a solution phase [13, 14]. The resulting redox reactions lead to alloying and dealloying processes that determine the composition and void formation in the final nanostructure. A similar mechanism is the Kirkendall effect that, based on the different diffusion rates of two metals at an interface, results in vacancy diffusion and subsequent void growth. Galvanic replacement and the Kirkendall effect often occur in the same process [15] and their combination can lead to complex nanostructures with multiple shells [16]. Conversion chemistry methods are mostly applied to colloidal nanoparticle solutions [17, 13, 18]. Nonetheless, many practical applications require the nanoparticles to be supported on a solid substrate. It is known that electromagnetic interaction of particles with a substrate can increase field enhancement and shift the plasmon resonance[19, 20]. In addition, anchoring the particles positions allows controlling their electromagnetic coupling and generating hot spots. The Langmuir-Blodgett technique is a common approach for obtaining a film of hollow nanoparticles on a substrate [21]. On the other hand, recent works have successfully demonstrated the direct application of galvanic replacement to templates consisting of nanoparticles deposited on a substrate [22, 23]. This possibility represents a very promising approach for fabrication of hollow nanostructures for it enables control of nanoparticle spatial arrangement before the conversion chemistry process takes place.

In this work we demonstrate the fabrication of hollow metal nanoparticle layers by galvanic replacement in Ag island films deposited on glass and silicon substrates. Metal islands films are appealing building blocks for cost-efficient and large-area production of plasmonic devices since they can be obtained by

well-established thin film techniques and their optical properties can be broadly tuned by adjusting the fabrication conditions [24, 25]. The characteristic large nanoparticle density and small interparticle distance makes these films efficient plasmonic sensors [26, 27]. Among noble metals, Ag shows the most prominent island growth in standard evaporation process. We show that increasing the concentration of the oxidizing agent ($HAuCl_4$) applied during the galvanic replacement yields a progressive surface plasmon resonance red-shift caused by composition, morphological and structural changes in the films. At large enough $HAuCl_4$ concentration, islands become hollow with multiple holes at their surface, boosting the sample sensitivity to refractive index changes. Therefore, the resulting structures are particularly attractive for sensing, one of the most actively investigated applications in plasmonics [28, 29, 30, 31].

2. Material and methods

The galvanic replacement reaction was done with the method of simple titration with a modified titration setup. During the reaction, deposited Ag islands were oxidized by $HAuCl_4$. This process is enabled by the redox potential difference between the $AuCl_4^-/Au$ (0.99 V vs. SHE) and AgCl/Ag (0.22 V vs. SHE) redox couple, according to the reaction:

$$3\,Ag(s) + HAuCl_4(aq) \rightarrow Au(s) + 3\,AgCl(s) + HCl(aq)$$

The Ag nanoparticles used as sacrificial template were deposited by electron beam evaporation in a modified Varian chamber using glass slides (VMR) and Si wafers (Si-Mat) as substrates. Samples on glass substrates were used for optical measurements and those on Si wafers were employed for electron microscopy analysis. The base pressure was 10^{-6} torr and the deposition rate was cca. 1 Å/s. Samples were deposited on substrates pre-heated at 200 °C and annealed for 1 hour at 300 °C in air after deposition in order to enhance island growth. The titration setup consists of a 50 mL beaker thermostated at 90 °C (±0.1 °C) in an oil bath. The temperature of the oil bath was measured with a Pt1000 temperature sensor. A sample holder (a Teflon grid) was placed inside the beaker, with a magnetic rod beneath it to obtain homogeneous titration solution. The oil bath was placed onto the magnetic stirer and the beaker was covered with a glass plate to prevent evaporation of the titration solution (see scheme in Figure S1 in Supplementary Information). First, 25 mL of milli Q water (MQW, 18 MΩ cm^{-1}) preheated to 90 °C was put into the beaker. After 5 minutes of thermostating, an aliquot of 100 μL of 2 mM aqueous solution of $HAuCl_4$ solution (titration solution in the manuscript) was added to the MQW. Titration was done at 90 °C to avoid AgCl formation on the islands surface. After 30 seconds of stirring of the titration solution at 1500 rpm, the sample was immersed into the solution. After 1 minute, the reaction was finished, sample was removed from the solution, washed with ethanol (HPLC grade, Sigma - Aldrich), dried under a stream of nitrogen and extinction spectrum was recorded with a UV-Vis Lambda 25 Perkin Elmer spectrophotometer equipped with deuterium and halogen lamps and using a quartz cuvette for measurements in liquid environment. Scanning electron microscopy (SEM) imaging

was done with a JEOL JSM 7000F microscope. Extended details on GISAXS measurements and modelling are given in the Supplementary Information.

The optical response of particles was computed using the boundary element method as implemented in the MNPBEM toolbox [32], that incorporates the classical Mie theory as well. Essentially, scalar and vector potentials are computed via boundary integrals of surface charge and current distributions resulting from boundary conditions of Maxwell's equations. Then, the electromagnetic field can be calculated at any point in space and the optical quantities of interest, such as the extinction cross section, can be computed. Optical constants from literature were used for the dielectric function of Au and Ag [33].

3. Results and discussion

The experimental procedure is schematically shown in Figure 1. First, 15 nm mass thickness Ag metal island films were deposited by electron beam evaporation on glass slides and silicon wafers. In order to enhance islands formation, film were deposited on substrates pre-heated at 200 °C and annealed at 300 °C for 1 hour at normal atmosphere after deposition. Afterwards, the samples were titrated in a beaker containing 25 ml of Milli-Q water and 100 μl of 2 mM aqueous solution of $HAuCl_4$. The sample was removed from the beaker after one minute, washed with ethanol and dried (see Experimental Section for additional details on the sample preparation). The process was repeated several times, using a new titration solution each time. Samples exposed more than 15 times to this process showed evident deterioration with the island film being removed from regions of the glass surface. Extinction measurements of samples deposited on glass substrates were taken after each titration process (lower panel in Figure 1). The untreated sample displays a peak centered at 465 nm corresponding to the localized dipole surface plasmon resonance of metal islands. The first titration step resulted in a blue-shift i.e. a shift to shorter wavelengths, of cca. 30 nm of this peak. Afterwards a continuous red-shift i.e. a shift to longer wavelengths took place, revealing an approximate linear dependence of the shift magnitude with the number of titrations or, equivalently, with the cumulative volume of 2 mM $HAuCl_4$ titration solution applied to the sample. Treatment with a total of 1500 μl of 2 mM $HAuCl_4$ titration solution volume resulted in a plasmon red-shift of nearly 300 nm with respect to the untreated sample. The origin of the observed blue and red shift of the plasmon resonance requires analyzing the islands compositional and morphological changes, as discussed below.

Scanning electron micrographs of metal island films were taken on samples treated with different total titration solution volume (Figure 2) in order to understand the optical properties evolution. The untreated sample presents a distribution of particles with different sizes and smooth contours, as expected for island films subjected to moderate thermal treatments [34]. Upon mild titration, islands start to display surface facetting, indicating the liquid-phase heteroepitaxial deposition of Au atoms on Ag [35, 36]. It corresponds to the first stage of galvanic replacement in which an Au shell is deposited on the nanoparticles surface as a consequence of Ag oxidization [14]. The deposition of

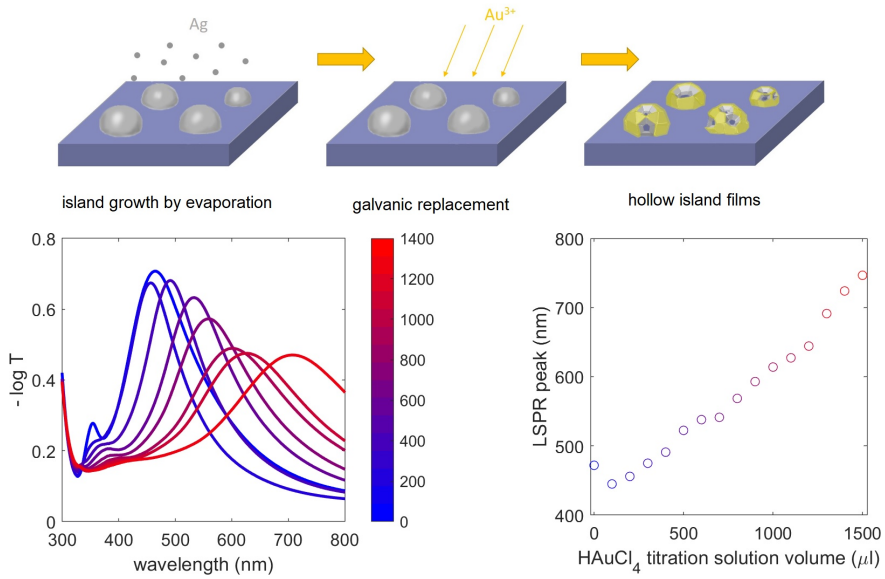

Figure 1: Top: scheme of the procedure for obtaining Ag hollow islands film by galvanic replacement. Down left: extinction spectra of Ag metal island films on glass substrates treated with different volumes of 2 mM $HAuCl_4$ titration solution. Down right: evolution of the surface plasmon resonance (LSPR) peak with the titration solution volume.

Au is also confirmed by gradual quenching of the extinction spectrum peak observed at 350 nm for the untreated sample. This peak corresponds to the islands quadrupole resonance that, as shown in the Supplementary Information (Figure S2) becomes strongly damped when a thin Au shell covers the Ag surface. Au shell formation should cause a red-shift of the dipole plasmon resonance. However, the initial stages of galvanic replacement are expected to take place preferentially at high surface energy sites such as defects and large curvature regions [36, 37]. Therefore, initial Au deposition can smooth out island irregular morphology while the particle surface may still show a predominant presence of Ag, which could explain the plasmon resonance blue shift observed after the first $HAuCl_4$ titrant addition. Additionally, the effect of temperature during the titration process may induce some slight particle reshaping towards larger sphericity which could also contribute to the mentioned shift.

Galvanic replacement studies on Ag colloids [14, 16] have shown that Ag-Au alloying and diffusion of Ag^+ into the bulk solution take place in parallel to Au deposition. A pinhole is eventually formed on the Au shell, enabling the process to continue by ion removal from the Ag core and leading to void nucleation, growth and propagation. At the final stage of galvanic replacement, Ag-Au dealloying results in the formation of nanocages and nanoframes and, finally, to complete shell fragmentation. A similar dynamics is observed in metal island films titrated with $HAuCl_4$. As the titration solution volume increases (third

panel in Figure 2), facetting becomes more evident and islands acquire a polyhedral shape. The appearance of pinholes on top of some Ag islands is visible in the electron micrographs (fourth panel in Figure 2). The pinhole morphology and size varies from island to island and reaches values of up to few nm at this titration stage. Besides black spots (pinholes), islands display dark-gray regions, i.e. regions with low electronic density, that point to voids formation inside the particle. For the largest titration solution volume (last panel in Figure 2), islands show multiple surface openings that reflect a nanoframe-like morphology. It is also possible to detect regions with shell fragments (see Figure S3 in the Supplementary information) indicating that at this stage some fraction of particles is already disintegrated and explaining why larger titration solution volumes resulted in film removal from the surface. Overall, the progressive Au deposition at first and the increase of island hollowness later, qualitatively explain the observed plasmon red-shift.

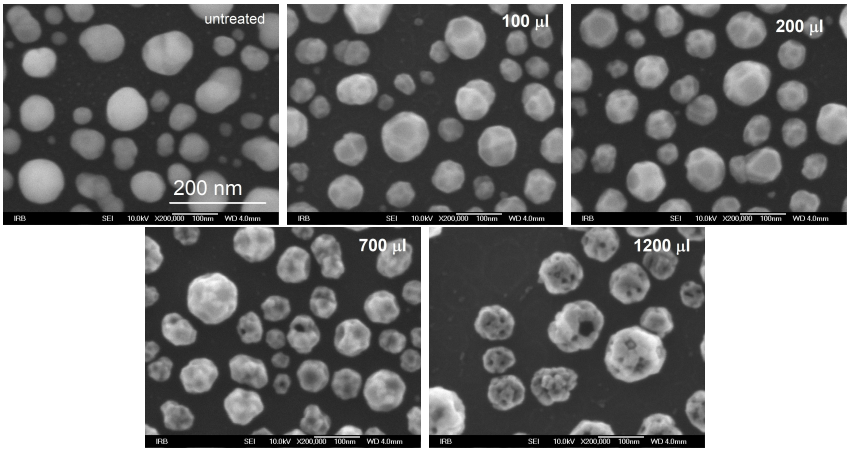

Figure 2: Electron micrographs of Ag island film on Si substrates treated with different 2 mM $HAuCl_4$ titration solution volumes: untreated, 100, 200, 700 and 1200 μl.

Besides morphological changes, it turns out that the islands spatial arrangement is also modified by titration, especially for large titration solution volumes. Thus, the last panel in Figure 2 and Figure S3 in the Supplementary Information show that some sample areas where no islands are present display a nearly circular faint halo. For lower titration solution volumes, the halo appears to be closely located to islands of similar dimensions (see Figure S3 in the Supplementary Information). It appears that morphological changes induced by titration enable islands to detach from the substrate and shift on it. In addition, micrographs showing larger areas evidence that the treated samples present zones with high island density and regions without islands, in contrast with the more homogeneous spatial arrangement of the untreated sample (Figure S4 in the Supplementary Information). This observation suggests that once the islands are able to detach from the substrate they tend to aggregate, in a similar way as

it happens in not-stabilized colloidal solutions, in order to reduce the particles surface energy. It should be taken into account that the larger electromagnetic coupling among islands that results from aggregation may represent a significant contribution to the modification of the optical properties and the observed plasmon red-shift [21]. It should be noted that closely located particle pairs (interparticle distance up to a couple of nm, according to SEM resolution) are observed even for untreated samples, but the number of these particle pairs in close proximity increases at large titration volumes. Therefore, the role of interparticle coupling in the overall plasmonic red-shift is expected to be enhanced for samples treated with largest volumes.

Samples were investigated by grazing incidence small angle X-ray scattering (GISAXS) at the Austrian SAXS beam line of the Synchrotron ELETTRA [38] (see Supplementary Information for experimental details). GISAXS gives information of relatively large areas (beam footprint up to a few mm^2) and therefore provides composition and morphological data statistically averaged over many particles, which is particularly advantageous in the case of metal island films [39]. Measured GISAXS scattering patterns are shown in the top panel in Figure 3. The experimental data were fitted by a model containing a reduced set of parameters able to describe changes due to the galvanic replacement process (Supplementary Information). Briefly, islands were assumed to consist of three spheroids representing an Ag core, Au shell and a hole within the Ag core, all with the same aspect ratio (Figure S5 in the Supplementary Information). The Ag shell was shifted towards the substrate to account for the Au deposition only on top and sides of the Ag core. Likewise, the hole spheroid was set to grow from top of the Ag core. The model was able to fit all the scattering patterns successfully (lower panel in Figure 3). The obtained morphology (insets in Figure 3 and Supplementary Information) confirms the gradual Au shell and hole growth with the titration solution volume. Additionally, the obtained size distribution showed a remarkable agreement with those deduced from electron micrographs, as shown in the Supplementary Information. It should be noted that the central part of the scattering patterns (small $|Q_y|$) was not fitted because the model neglects the spatial correlation among islands and only the form factor, i.e individual island morphology, was taken into account. Yet, a close inspection of the scattering patterns reveals that the untreated sample displays two symmetric peaks around $Q_y = 0$, reflecting a preferential interparticle distance [40]. These peaks disappear on treated samples, in line with the islands spatial rearrangement discussed above.

The sensing potential of hollow metal island films was determined by extinction spectra measurements with the samples immersed in a quartz cuvette that was either empty or filled with ethanol (Figure 4 and Table 1). The plasmon peak of the untreated sample shows a wavelength shift of 33 nm that corresponds to a refractive index sensitivity factor (SF) of 92 nm per refractive index unit (RIU), in agreement with typical values for metal island films [41]. Similar SF values are obtained for samples treated with titration solution volumes up to 700 μl. In fact, a slight drop in the refractive index sensitivity (SF = 72 nm/RIU) can be noticed for titration solution volumes around 200 μl. SF

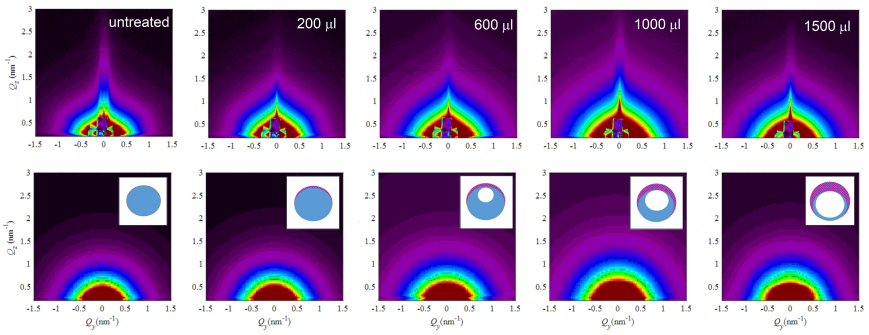

Figure 3: GISAXS scattering pattern measured (top panel) and modeled (bottom panel) for metal island films on glass subjected to different $HAuCl_4$ titration solution volumes. The patterns show the scattered intensity as a function of the scattering wave vector $\vec{q}$ in the z (perpendicular to the sample surface, Q_z) and y (parallel to the sample surface, Q_y) directions. The modulus of $\vec{q}$ is $4\pi \sin\theta/\lambda$, where 2θ is the X-ray scattering angle. Insets in the modeled data show the obtained particle morphology.

increases to 114 nm/RIU at 700 μl. Afterwards, a strong sensitivity increase is observed, reaching a wavelength shift of 129 nm (SF = 360 nm/RIU) for the sample treated with the largest titration solution volume. Thus, galvanic replacement on metal islands film yields a 4-fold enhancement of the refractive index sensitivity. Since the plasmon resonance in titrated samples is broader than in untreated samples, the figure of merit (FOM) increase is lesser (ca. 2.5 times) than the sensitivity improvement.

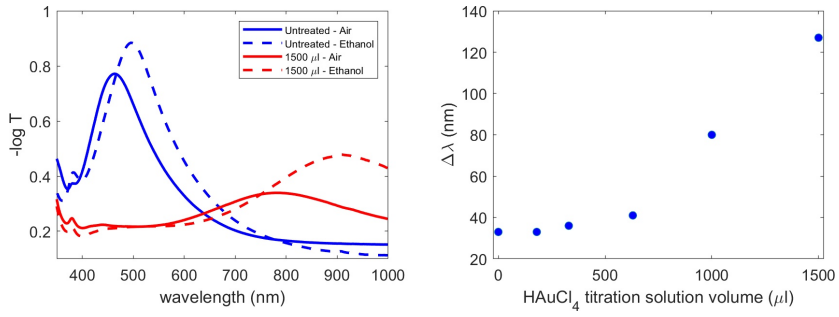

Figure 4: Left: Extinction spectra of an Ag metal island film sample on glass substrate: untreated and treated with 1500 μl of 2mM $HAuCl_4$ titration solution, in air and ethanol. Right: evolution of the localized surface plasmon resonance peak shift when samples are placed in ethanol as a function of the titration solution volume.

In order to explain the dependence of the refractive index sensitivity on the applied titration solution volume, the electrodynamics response of particles with sizes based on characterization results was computed (Figure 5). SF was calculated by simulating extinction spectra for different refractive index values of the medium embedding the particle. This approach neglects that particles

Volume (μL)	$\Delta\lambda$ (nm)	SF (nm/RIU)	FWHM (nm)	FOM
0	33	92	165	0.56
180	26	72	198	0.36
330	33	92	170	0.54
630	41	114	192	0.59
1000	82	229	227	1.01
1500	129	360	263	1.37

Table 1: Refractive index sensor characteristics ($\Delta\lambda$ - wavelength shift of the plasmon resonance when the sample is placed in ethanol instead of air, SF - sensitivity factor: wavelength shift per refractive index unit, FWHM - full width at half maximum of the plasmon resonance, FOM - figure of merit: SF/FWHM) for samples treated with different titration solution volumes.

are supported and the effective embedding medium is partially determined by the substrate. However, for light polarization parallel to the sample surface - like in the case of extinction measurements at normal incidence - the effect of a glass substrate is weak [42] and results in a moderate SF decrease [19]. For the case of a solid Ag particle (first column in Figure 5), the computed SF is significantly higher than the one experimentally determined for untreated samples. Nonetheless, it should be noted that the islands are not covered and direct exposition to air decreases Ag plasmonic performance due to its reactivity. The SF of Au particles (second column) is lower than for Ag and comparable to those measured for islands treated with small titration solution volumes. Therefore, the experimentally observed slight SF decrease can be related to the shell formation that, even when very thin, grants the Au character to the island plasmonic properties (Figure S2 in Supplementary information). Void growth inside an Au sphere (third column) enables electromagnetic coupling between cavity and sphere modes according to the plasmon hybridization model [4] and improves the SF, explaining the mild sensitivity increase from low to moderate titration solution volumes. In order to explain the strong sensitivity increase for solution volumes above 700 μl, the presence of a pinhole on the particle top (fourth column) and, especially, of multiple holes on the particle sides has to be taken into account (fifth column). It has been reported that the presence of surface openings is critical to boost the sensitivity of hollow nanoparticles [5] due to the surface charge redistribution on the regions around the pinholes [43] and the larger available contact surface between particle and embedding medium. Yet, in order to obtain SF values close to the one measured for the sample treated with 1500 μl the pinhole size needs to be much larger than the one suggested by electron micrographs. A more plausible explanation for the discrepancy between calculated and measured SF is the enhanced electromagnetic coupling among particles caused by islands aggregation. Thus, a dimer of particles with multiple pinholes, separated 5 nm and excited with light polarized along the dimer axis (sixth column) has a SF cca. 30% larger than for a single particle. It turns out that the islands spatial re-arrangement that results from galvanic replacement is relevant for sensitivity increase. In a similar fashion, restructuring of metal

island films as a result of their interaction with proteins has been previously observed. This adaptability phenomenon was exploited to increase the island films sensitivity to the Raman signal of these proteins caused by the increase of hot spots sites [44, 27].

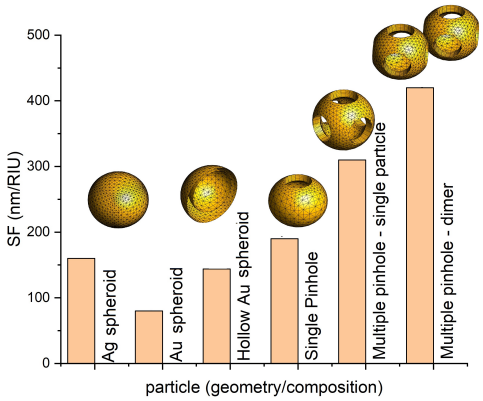

Figure 5: Sensitivity factor (plasmon resonance wavelength change per refractive index unit change of the surrounding medium) for different spheroidal particles with dimensions and geometry extracted from GISAXS and electron micrographs results. On top of each bar a sketch of the particles used in the computations is shown (for the core-shell particle, only half particle is shown in order to display the core).

4. Conclusion

In summary, it has been shown that standard galvanic replacement procedures used for obtaining colloidal solutions of hollow nanoparticles can be applied to the formation of hollow metal islands films supported on solid substrates. Modifications resulting from galvanic replacement processes are analogous to those observed in colloidal solutions: Au growth on islands surface, void nucleation inside particles and formation of nanocage and nanoframe-like structures. In addition, the film spatial arrangement is varied as islands become more aggregated. Morphological and structural changes result in a plasmon red-shift and increased refractive index sensitivity. In the case of samples treated with large $HAuCl_4$ titration solution volumes the sensitivity is enhanced four times (360 nm/RIU vs 92 nm/RIU) and the figure of merit two and a half times (1.37 vs 0.56) in comparison with the untreated samples. Overall, the study demonstrates that the combination of well-established conversion chemistry procedures with standard thin film fabrication techniques opens a new path to the design and fabrication of highly effective plasmonic sensors.

5. Acknowledgments

The authors thank the financial support of the Croatian Science Foundation through the grant number IP-2019-04-5424.

References

References

[1] X. Wang, J. Feng, Y. Bai, Q. Zhang, Y. Yin, Synthesis, properties, and applications of hollow micro-/nanostructures, Chemical reviews 116 (18) (2016) 10983–11060.

[2] X. W. Lou, L. A. Archer, Z. Yang, Hollow micro-/nanostructures: synthesis and applications, Advanced Materials 20 (21) (2008) 3987–4019.

[3] S. F. Soares, T. Fernandes, A. L. Daniel-da Silva, T. Trindade, The controlled synthesis of complex hollow nanostructures and prospective applications, Proceedings of the Royal Society A 475 (2224) (2019) 20180677.

[4] E. Prodan, C. Radloff, N. J. Halas, P. Nordlander, A hybridization model for the plasmon response of complex nanostructures, science 302 (5644) (2003) 419–422.

[5] A. Genç, J. Patarroyo, J. Sancho-Parramon, N. G. Bastús, V. Puntes, J. Arbiol, Hollow metal nanostructures for enhanced plasmonics: synthesis, local plasmonic properties and applications, Nanophotonics 6 (1) (2017) 193–213.

[6] J. Z. Zhang, Biomedical applications of shape-controlled plasmonic nanostructures: a case study of hollow gold nanospheres for photothermal ablation therapy of cancer, The Journal of Physical Chemistry Letters 1 (4) (2010) 686–695.

[7] J. You, G. Zhang, C. Li, Exceptionally high payload of doxorubicin in hollow gold nanospheres for near-infrared light-triggered drug release, ACS nano 4 (2) (2010) 1033–1041.

[8] J. Chen, F. Saeki, B. J. Wiley, H. Cang, M. J. Cobb, Z.-Y. Li, L. Au, H. Zhang, M. B. Kimmey, X. Li, et al., Gold nanocages: bioconjugation and their potential use as optical imaging contrast agents, Nano letters 5 (3) (2005) 473–477.

[9] Y. Sun, Y. Xia, Increased sensitivity of surface plasmon resonance of gold nanoshells compared to that of gold solid colloids in response to environmental changes, Analytical chemistry 74 (20) (2002) 5297–5305.

[10] A. M. Schwartzberg, T. Y. Oshiro, J. Z. Zhang, T. Huser, C. E. Talley, Improving nanoprobes using surface-enhanced raman scattering from 30-nm hollow gold particles, Analytical chemistry 78 (13) (2006) 4732–4736.

[11] J. Zeng, Q. Zhang, J. Chen, Y. Xia, A comparison study of the catalytic properties of au-based nanocages, nanoboxes, and nanoparticles, Nano letters 10 (1) (2010) 30–35.

[12] Q. Zhang, W. Wang, J. Goebl, Y. Yin, Self-templated synthesis of hollow nanostructures, Nano Today 4 (6) (2009) 494–507.

[13] Y. Sun, B. T. Mayers, Y. Xia, Template-engaged replacement reaction: a one-step approach to the large-scale synthesis of metal nanostructures with hollow interiors, Nano Letters 2 (5) (2002) 481–485.

[14] X. Xia, Y. Wang, A. Ruditskiy, Y. Xia, 25th anniversary article: Galvanic replacement: a simple and versatile route to hollow nanostructures with tunable and well-controlled properties, Advanced Materials 25 (44) (2013) 6313–6333.

[15] S. W. Chee, S. F. Tan, Z. Baraissov, M. Bosman, U. Mirsaidov, Direct observation of the nanoscale kirkendall effect during galvanic replacement reactions, Nature communications 8 (1) (2017) 1–8.

[16] E. González, J. Arbiol, V. F. Puntes, Carving at the nanoscale: sequential galvanic exchange and kirkendall growth at room temperature, Science 334 (6061) (2011) 1377–1380.

[17] S. E. Skrabalak, J. Chen, Y. Sun, X. Lu, L. Au, C. M. Cobley, Y. Xia, Gold nanocages: synthesis, properties, and applications, Accounts of chemical research 41 (12) (2008) 1587–1595.

[18] A. Ruditskiy, Y. Xia, The science and art of carving metal nanocrystals, ACS nano 11 (1) (2017) 23–27.

[19] M. A. Mahmoud, M. A. El-Sayed, Substrate effect on the plasmonic sensing ability of hollow nanoparticles of different shapes, The Journal of Physical Chemistry B 117 (16) (2013) 4468–4477.

[20] Y.-F. Chau, Z.-H. Jiang, Plasmonics effects of nanometal embedded in a dielectric substrate, Plasmonics 6 (3) (2011) 581–589.

[21] M. Mahmoud, M. El-Sayed, Aggregation of gold nanoframes reduces, rather than enhances, sers efficiency due to the trade-off of the inter-and intraparticle plasmonic fields, Nano letters 9 (8) (2009) 3025–3031.

[22] M. Hajfathalian, K. D. Gilroy, S. D. Golze, A. Yaghoubzade, E. Menumerov, R. A. Hughes, S. Neretina, A wulff in a cage: the confinement of substrate-based structures in plasmonic nanoshells, nanocages, and nanoframes using galvanic replacement, ACS nano 10 (6) (2016) 6354–6362.

[23] S. Neretina, R. A. Hughes, K. D. Gilroy, M. Hajfathalian, Noble metal nanostructure synthesis at the liquid–substrate interface: new structures, new insights, and new possibilities, Accounts of chemical research 49 (10) (2016) 2243–2250.

[24] O. Stenzel, Metal island films, in: Optical Coatings, Springer, 2014, pp. 279–315.

[25] J. Sancho-Parramon, V. Janicki, H. Zorc, On the dielectric function tuning of random metal-dielectric nanocomposites for metamaterial applications, Optics express 18 (26) (2010) 26915–26928.

[26] T. A. Bendikov, A. Rabinkov, T. Karakouz, A. Vaskevich, I. Rubinstein, Biological sensing and interface design in gold island film based localized plasmon transducers, Analytical chemistry 80 (19) (2008) 7487–7498.

[27] V. P. Drachev, M. D. Thoreson, V. M. Shalaev, Sensing proteins with adaptive metal nanostructures, in: Surface Plasmon Nanophotonics, Springer, 2007, pp. 197–215.

[28] M. Butt, S. Khonina, N. Kazanskiy, Plasmonics: A necessity in the field of sensing-a review, Fiber and Integrated Optics 40 (1) (2021) 14–47.

[29] W. Fan, B. J. Lawrie, R. C. Pooser, Quantum plasmonic sensing, Physical Review A 92 (5) (2015) 053812.

[30] Y.-F. C. Chau, C.-T. C. Chao, H.-P. Chiang, C. M. Lim, N. Y. Voo, A. H. Mahadi, Plasmonic effects in composite metal nanostructures for sensing applications, Journal of Nanoparticle Research 20 (7) (2018) 1–13.

[31] Y.-F. Chou Chau, K.-H. Chen, H.-P. Chiang, C. M. Lim, H. J. Huang, C.-H. Lai, N. Kumara, Fabrication and characterization of a metallic–dielectric nanorod array by nanosphere lithography for plasmonic sensing application, Nanomaterials 9 (12) (2019) 1691.

[32] U. Hohenester, A. Trügler, Mnpbem–a matlab toolbox for the simulation of plasmonic nanoparticles, Computer Physics Communications 183 (2) (2012) 370–381.

[33] P. B. Johnson, R.-W. Christy, Optical constants of the noble metals, Physical review B 6 (12) (1972) 4370.

[34] K. Aslan, Z. Leonenko, J. R. Lakowicz, C. D. Geddes, Annealed silver-island films for applications in metal-enhanced fluorescence: interpretation in terms of radiating plasmons, Journal of fluorescence 15 (5) (2005) 643–654.

[35] A. S. Preston, R. A. Hughes, T. B. Demille, V. M. R. Davila, S. Neretina, Dewetted nanostructures of gold, silver, copper, and palladium with enhanced faceting, Acta Materialia 165 (2019) 15–25.

[36] K. D. Gilroy, P. Farzinpour, A. Sundar, T. Tan, R. A. Hughes, S. Neretina, Substrate-based galvanic replacement reactions carried out on heteroepitaxially formed silver templates, Nano Research 6 (6) (2013) 418–428.

[37] Y. Sun, Y. Xia, Mechanistic study on the replacement reaction between silver nanostructures and chloroauric acid in aqueous medium, Journal of the American Chemical Society 126 (12) (2004) 3892–3901.

[38] H. Amenitsch, M. Rappolt, M. Kriechbaum, H. Mio, P. Laggner, S. Bernstorff, First performance assessment of the small-angle x-ray scattering beamline at elettra, Journal of synchrotron radiation 5 (3) (1998) 506–508.

[39] M. Buljan, M. Karlušić, N. Nekić, M. Jerčinović, I. Bogdanović-Radović, S. Bernstorff, N. Radić, I. Mekterović, Gisaxs analysis of ion beam modified films and surfaces, Computer Physics Communications 212 (2017) 69–81.

[40] P. Müller-Buschbaum, A basic introduction to grazing incidence small-angle x-ray scattering, in: Applications of synchrotron light to scattering and diffraction in materials and life sciences, Springer, 2009, pp. 61–89.

[41] T. Karakouz, D. Holder, M. Goomanovsky, A. Vaskevich, I. Rubinstein, Morphology and refractive index sensitivity of gold island films, Chemistry of Materials 21 (24) (2009) 5875–5885.

[42] C. Noguez, Surface plasmons on metal nanoparticles: the influence of shape and physical environment, The Journal of Physical Chemistry C 111 (10) (2007) 3806–3819.

[43] Y.-F. Chau, C.-Y. Jheng, Buried effects of surface plasmon resonance modes for periodic metal–dielectric nanostructures consisting of coupled spherical metal nanoparticles with cylindrical pore filled with a dielectric, Plasmonics 9 (1) (2014) 1–9.

[44] V. P. Drachev, M. D. Thoreson, E. N. Khaliullin, V. J. Davisson, V. M. Shalaev, Surface-enhanced raman difference between human insulin and insulin lispro detected with adaptive nanostructures, The Journal of Physical Chemistry B 108 (46) (2004) 18046–18052.